Published in final edited form as:

J Neurochem. 2017 August ; 142(3): 365–377. doi:10.1111/jnc.14069.

Heterogeneous Extracellular Dopamine Regulation in the Subregions of the Olfactory Tubercle

Jinwoo Park[1,2,4], **Ken T. Wakabayashi**[1,3], **Caitlin Szalkowski**[1], **Rohan V. Bhimani**[4]

[1]Department of Biotechnical and Clinical Laboratory Sciences

[2]Pharmacology and Toxicology

[3]Research Institute in Addictions

[4]Neuroscience Program, Jacobs School of Medicine and Biomedical Sciences, University at Buffalo, State University of New York, Buffalo, 14214, USA

Abstract

Recent studies show that dense dopamine (DA) innervation from the ventral tegmental area (VTA) to the olfactory tubercle (OT) may play an important role in processing multisensory information pertaining to arousal and reward, yet little is known about DA regulation in the OT. This is mainly due to the anatomical limitations of conventional methods to determine DA dynamics in small heterogeneous OT subregions located in the ventral most part of the brain. Additionally, there is increasing awareness that anteromedial and anterolateral subregions of the OT have distinct functional roles in natural and psychostimulant drug reinforcement as well as regulating other types of behavioral responses such as aversion. Here, we compared extracellular DA regulation (release and clearance) in three subregions (anteromedial, anterolateral, and posterior) of the OT of urethane-anesthetized rats using *in vivo* fast-scan cyclic voltammetry following electrical stimulation of VTA dopaminergic cell bodies. The neurochemical, anatomical, and pharmacological evidence confirmed that the major electrically evoked catecholamine in the OT was DA across both its anteroposterior and mediolateral extent. While both D2 autoreceptors and DA transporters play important roles in regulating evoked DA in OT subregions, DA in the anterolateral OT was regulated less by the D2 receptors when compared to other OT subregions. Comparing previous data of other DA rich ventral striatum regions, the slow DA clearance across the OT subregions may lead to a high extracellular DA concentration and contribute towards volume transmission. These differences in DA regulation in the terminals of OT subregions and other limbic structures will help us understand the neural regulatory mechanisms of DA in the OT, which may elucidate its distinct functional contribution in the ventral striatum towards mediating aversion, reward and addiction processes.

Keywords

olfactory tubercle; dopamine; dopamine D2 receptors; dopamine transporters; fast-scan cyclic voltammetry; ventral tegmental area

Corresponding Author: Jinwoo Park, Ph.D., Clinical Laboratory Sciences, 26 Cary Hall, 3435 Main St., University at Buffalo, Buffalo, NY, 14214-3005, USA, Tel : +1 (716) 829-5186, Fax : +1 (919) 829-3601, jinwoopa@buffalo.edu.

Introduction

The olfactory tubercle (OT) has long been considered as an olfactory area because it receives input from the olfactory bulb (Wesson & Wilson 2011). However, this view has begun to change with data indicating that the OT also functions as a distinct component of the limbic system. Recent findings have suggested that the OT, in addition to processing odor input, also serves to integrate reward and motivation information from other limbic structures (Ikemoto 2003, Ikemoto 2007, Wesson & Wilson 2011, Shin *et al.* 2010, Gadziola & Wesson 2016). Anatomically, the OT is a substructure of the ventral striatum, a brain region which also includes the nucleus accumbens (NAc) and is adjacent to the ventral pallidum (VP), a distinct structure which receives primary output from the ventral striatum (Alheid & Heimer 1988, Wesson & Wilson 2011). Although the OT has been often considered as a ventral extension of the larger NAc, growing evidence suggests that the OT is a distinct component of the ventral striatum, taking into account its morphology, chemistry, and anatomical connectivity (Ikemoto 2007, Wesson & Wilson 2011, Millhouse & Heimer 1984). Unlike the NAc, the OT has a trilaminar structure containing distinct layers of neurons and is interconnected with numerous brain regions including neighboring cognitive and reward-related limbic structures such as the NAc and VP as well as the olfactory bulb, the prefrontal cortex, thalamus and hippocampus (Shin et al. 2010, Wesson & Wilson 2011, Giessel & Datta 2014). Additionally, while the OT, like the NAc, is comprised mainly of GABAergic medium spiny neurons expressing D1 and D2 DA receptors and receives dense DA inputs from the ventral tegmental area (VTA) (Voorn *et al.* 1986), the anatomical distribution of the VTA DA inputs to the OT and their function may differ from that of the NAc (Ikemoto 2007, Murata *et al.* 2015).

The OT can be subdivided into several subregions, including the anteromedial (amOT), anterolateral (alOT), and posterior (pOT) subregions. The regional specificity may also extend to distinct subpopulations of VTA DA innervation of the OT, as the medial part of the VTA projects to the medial ventral striatum, including the medial OT, while the lateral VTA projects more to the lateral OT (Ikemoto 2007). Therefore, heterogeneous DA inputs into the OT may be an important and distinct contributor to how the limbic system processes reward and arousal-related information. Indeed, recent data has suggested that the different OT subregions can be functionally distinct with regard to both natural (DiBenedictis *et al.* 2015, Murata et al. 2015, Agustin-Pavon *et al.* 2014) and stimulant reward (Ikemoto 2007). In light of these new findings, the OT has recently become a focus of increased interest as a key processing area for DA associated with drug reward and goal directed behavior, perhaps distinct from other parts of the ventral striatum (Ikemoto 2007, DiBenedictis et al. 2015, Gadziola & Wesson 2016, Robinson *et al.* 2005).

However, little is known about how extracellular DA is regulated in the OT overall and whether DA is regulated heterogeneously in the subregions of the OT. In part, this is due to the challenges in selectively monitoring DA transmission in the OT apart from adjacent DA rich areas such as the NAc, VP or caudate putamen (CPu) with conventional *in vivo* neurochemical methods including microdialysis. In addition, the rat OT has appreciable amounts of DA in an area only a few hundred microns across and is located in the ventral

most portion of the brain, which makes selective monitoring of DA in the OT a challenge. In this study, we employed fast-scan cyclic voltammetry (FSCV) coupled with carbon-fiber microelectrodes; a technique that has been widely used to study the regulatory mechanisms of subsecond changes of many neurochemicals such as monoamines and adenosine in discrete brain regions, including an initial characterization of the OT (Bucher & Wightman 2015, Robinson *et al.* 2008, Swamy & Venton 2007, Park *et al.* 2015, Robinson *et al.* 2002, Robinson & Wightman 2004, Robinson et al. 2005). We hypothesize that this approach having high spatial (≤ 100 μm) as well as temporal (≤ 100 ms) resolution allows us to overcome the limits associated with conventional neurochemical techniques to study distinct extracellular DA regulation in the subregions of the OT. Importantly, unlike the initial studies characterizing the OT in behaving rats (Robinson & Wightman 2004, Robinson et al. 2002), we used an anesthetized approach to accurately assess the mechanisms of DA regulation (i.e. release and clearance) in OT subregions, avoiding confounding issues present in awake behaving rats, such as affective and motivational states and the presence of contextual cues at the time of recording.

Here, as an extension of our recent work and others (Wakabayashi *et al.* 2016, Robinson et al. 2005), we identified for the first time the major catecholamine evoked in the OT by the electrical stimulation of the VTA as DA and subsequently determined how the regulation of extracellular DA release and clearance differed in the amOT, alOT and pOT with pharmacological manipulation.

Materials and methods

Animals

Adult male Sprague-Dawley rats (290–400g) were purchased from Charles River Laboratories (Wilmington, MA, USA) and housed in temperature and humidity controlled rooms with a 12 hours on/off light cycle (lights on at 6:00 am). Food and water were available *ad libitum*. All procedures for handling and caring for laboratory animals were in accordance with the “Guide for Care and Use of Laboratory Animals” (8th Edition, 2011, US National Research Council) and were approved by the Institutional Animal Care and Use Committee of the University at Buffalo.

Surgery

Rats were anesthetized with urethane (1.5 g/kg) and placed in a stereotaxic frame (David Kopf Instruments, Tujunga, CA). Temperature was maintained at 37 ºC with a heating pad (Harvard Apparatus, Holliston, MA). The scalp was depilated, and swabbed with iodine and ethanol. Pre-incision local anesthesia was induced by an injection of bupivacaine (1.6 mg/kg s.c.), the dorsal skull surface was exposed, and small holes were drilled in the skull for implanting the carbon-fiber microelectrodes as described in previous studies (Park et al. 2015, Park *et al.* 2011). Each rat received one carbon-fiber microelectrode implant in the anteromedial OT (amOT; from bregma, AP +1.8 mm, ML +0.9 mm, DV from −7.8 to −8.4 mm), anterolateral OT (alOT; AP +1.8 mm, ML +2.5 mm, DV from −8.3 to −8.8 mm) or posterior OT (pOT; AP −0.1 mm, ML +2.5 mm, DV from −8.5 to −9.8 mm), according to coordinates of Paxinos and Watson (Paxinos & Watson 2007). For simultaneous

measurements, another microelectrode was implanted in one of the other subregions of the OT. During the same surgery, ipsilateral holes were drilled for the bipolar stimulating electrode above the VTA (AP −5.2 mm, ML +1.0, DV −8.0 mm to −9.0 mm). A Ag/AgCl reference electrode was placed into the contralateral hemisphere and was secured on the skull with dental cement.

Electrical stimulation

Electrical stimulation was accomplished with a bipolar, stainless-steel electrode (0.2 mm diameter, Plastics One, Roanoke, VA). The stimulating electrode insulated to the tip (separated by ~ 1.0 mm) was placed into the VTA/substantia nigra (SN). Stimulus pulses were computer-generated with a 6711 PCI card (National Instruments, Austin, TX, USA) and were electrically isolated from the electrochemical system (NL 800A, Neurolog, Medical Systems Corp., Great Neck, NY, U.S.A.). The electrical stimulation consisted of biphasic square wave pulses (300 μA, 2 ms/ each phase) with stimulation frequencies between 5 and 60 Hz. The number of stimulus pulses was normally held constant at 60. Each stimulation was repeated every 4 or 5 min to allow time for releasable DA stores to return to their original levels, which generate reproducible responses for DA release (Kita *et al.* 2007).

Voltammetric procedures for dual measurement

Glass-encased cylindrical carbon-fiber microelectrodes were prepared as described earlier (Cahill & Wightman 1995). T-650 untreated carbon fibers (Thornel, Amoco Corp., Greenville, SC) with an exposed length of 75 – 100 μm and 7 μm nominal diameter were used (Wakabayashi et al. 2016). FSCV was computer-controlled and the experimental setup for dual measurement has been described previously (Park et al. 2011, Zachek *et al.* 2010). TH-1 software was used with a Quad UEI instrument that has four independent current transducers and can support four different carbon-fiber microelectrodes (Department of Chemistry Electronic Shop, University of North Carolina at Chapel Hill). Two carbon-fiber microelectrodes were referenced to the sole reference electrode. A triangular scan (−0.4 to +1.3 V, 400 V/s) was simultaneously applied to both electrodes and repeated every 100 ms. The triangular waveform was low-pass filtered at 2 kHz to remove digitization noise and data were digitized and processed using NI-6711 and NI-6251 DAC/ADC cards and TH-1. Cyclic voltammograms obtained during electrical stimulation were background subtracted digitally from those collected during baseline recording. Temporal responses were determined by monitoring the current at the peak oxidation potential for DA in successive voltammograms. As the carbon-fiber microelectrode was used to generate a lesion for histological verification, detailed below, the average post-calibration factor (9.2 ± 1.1 pA/($\mu M \cdot \mu m^2$) was obtained *in vitro* with known concentrations of DA from our recent study (n = 8 electrodes) to determine DA concentrations in the OT (Wakabayashi et al. 2016).

Histology

At the end of experiments, a lesion was made at the recording site by applying continuous current (20 μA for 10 s) to carbon-fiber microelectrodes to verify microelectrode placements in the OT (Wakabayashi et al. 2016, Park et al. 2015). This precluded post-calibration of the electrode sensitivity. Brains were removed from the skull, stored in 10 % formaldehyde for

at least 3 days, and sectioned into 40–50 μm coronal sections. The sections were mounted on slides and viewed under a light microscope.

Drugs and reagents

All chemicals and drugs were obtained from Sigma-Aldrich (St. Louis, MO, USA) unless otherwise indicated. *In vitro* post-calibration of carbon-fiber microelectrodes was performed in a Tris buffer solution at a pH 7.4 containing 15 mM Tris, 140 mM NaCl, 3.25 mM KCl, 1.2 mM $CaCl_2$, 1.25 mM NaH_2PO_4, 1.2 mM $MgCl_2$, and 2.0 mM Na_2SO_4 in double distilled water (Mega Pure System, Corning Glasswork, Corning, NY) using a flow cell as described in previous studies (Robinson & Wightman 2007). Desipramine-HCl, raclopride-HCl, and idazoxan-HCl were dissolved in saline. GBR 12909-HCl was dissolved in double distilled water and then diluted with saline. Their effects on catecholamines and the doses used in this study are based on previous data (Park *et al.* 2009, Park et al. 2011, Fox & Wightman 2017, Herr *et al.* 2012, Budygin *et al.* 2000, Rice & Patel 2015), and a subset of rats used in this study (n = 26) received a random pair of drugs (i.e. α_2 receptor inhibitor followed by the selective NET inhibitor or D2 autoreceptor inhibitor followed by DAT inhibitor) that were systemically administered. All drugs were given intraperitoneally (i.p.) and injected volumes were 0.6 ml/kg.

Statistical analysis

Voltammetric data are presented as color plots where abscissa represents time, ordinate represents potential, and current is encoded in false color (Michael *et al.* 1999). Clampfit 8.1 as part of the pCLAMP 8.1 software package (Axon Instruments, Foster City, CA) was used to analyze electrically evoked maximal DA concentration ($[DA]_{max}$), the rise time (t_r), the time from the signal onset to the point the maximum is reached of $[DA]_{max}$, and the half-life ($t_{1/2}$) for DA clearance, the time to descend from its maximum value to half of that value (Park *et al.* 2006, Park et al. 2011). Naturally occurring DA releases (termed “transients”) were defined as signals that were greater than five times the root-mean-square noise level and were analyzed for frequency and amplitude using Mini Analysis Software (Synaptosoft, Decatur, GA, USA) (Park *et al.* 2010). While simultaneous measurements in the same animal eliminate experimental confounds such as variable levels of anesthesia and allow direct comparison of neurotransmitter dynamics under identical conditions (Park et al. 2011, Park et al. 2015, Zachek et al. 2010), the success rate of such measurements (~60 %) was lower than for single measurements. Therefore, data in this study were pooled from both single and simultaneous dual measurements. The effects of drugs were expressed as % of change from pre-drug baseline. Data were analyzed in Prism (GraphPad Software version 6.0, La Jolla, CA. USA) where one-sample t-tests (Fig. 2(c)&(d), one-way (Table 1 and 2), and two-way repeated measures ANOVA (Figs 2(c)&(d) and 5(c)&(d)) were used to determine statistical significance, followed by a Fisher post-hoc test, where appropriate. The criterion of significance was set at $p < 0.05$. Data from 37 rats were analyzed for this study. Group selection was not randomized. Rats were arbitrarily assigned their OT recording locations as well as the drug pair administered. Initial analysis of drug effects was conducted by an experimenter blind to both the brain region and drugs administered. The sample sizes of experiments were determined based on our previous studies without *a priori* power calculations (Wakabayashi et al. 2016, Park et al. 2011, Park et al. 2015). No data were

excluded for the statistical analysis except if histological examination revealed that the carbon-fiber electrode was anatomically off-target. Data are represented as mean ± S.E.M. and '*n*' values indicating the number of rats.

Results

Mapping electrically evoked catecholamine release in the subregions of the OT.

Catecholamine release in the amOT, alOT, and pOT subregions evoked by electrical stimulation of the VTA/SN (60 Hz, 60 pulses) was mapped at different depths to characterize the distribution of catecholamine release sites in each subregion. For this portion of the study, the stimulating electrode was fixed in the VTA/SN at a depth where maximal catecholamine release, $[CA]_{max}$, was observed in the OT. When the stimulating electrode was above or below the VTA/SN, catecholamine release in the OT was not observed. Figure 1 (top left panels, (a)-(c)) shows the coronal plane where measurements were made in the different OT subregions where the approximate carbon-fiber microelectrode track is shown by the dotted line.

Electrically evoked catecholamine release was measured as the carbon-fiber microelectrodes were lowered incrementally beginning at 5.0 or 6.0 mm from the skull (i.e. the CPu or NAc), and were taken 200 – 300 μm apart. As the electrode approached the OT, measurements were carefully made every 100 μm. Representative evoked release at different depths (Fig. 1(d)-(f)) showed robust catecholamine release when the carbon-fiber microelectrodes were in the NAc and CPu, where the major catecholamine is DA (Park et al. 2010, Park et al. 2009). As the electrode transited through the ventral region of the NAc and VP, evoked release markedly decreased before reappearing robustly when the electrodes reached the OT, peaking in the ventral most part of the OT near the border of the brain near the ventral skull. The voltammograms of evoked signals in the subregions of the OT (insets in Fig. 1) are identical to the voltammograms of catecholamines like DA, with an oxidation to its *ortho*-quinone form at ~+0.6 – +0.7 V and a reduction back to DA at ~ −0.2 – −0.3 V, observed in the NAc and CPu. Each individual recording evidenced this pattern, and was seen in the average relative response, clearly delineating two spatially distinct areas (Fig. 1 top right panels, (a)-(c)).

Plots of the evoked catecholamine release were normalized to the maximum value observed along the track of the electrodes. The maximal relative response of catecholamine in the OT was 0.79 ± 0.09 (amOT), 0.90 ± 1.0 (alOT), and 0.74 ± 0.08 (pOT). All values were similar or greater than that of catecholamine release observed in the adjacent NAc (0.69 ± 0.07) or CPu (0.57 ± 0.18), respectively, although this difference was not significant ($p > 0.05$). Notably, the ventral-most evoked catecholamine was observed in a relatively narrow region only ~500 μm across, which corresponds with the anatomical thickness of the rat OT. Lowering the electrodes further resulted in a rapid decrease in evoked DA signal, finally causing them to break against the ventral skull within ~200 μm. These observations suggested that this restricted region of electrically evoked catecholamine represented the OT and not a neighboring but much larger DA-rich limbic structure such as the NAc or CPu. A representative histological section with the post-experiment electrolytic lesion highlighted in red dotted circle. (Supplementary Fig. 1)

Effects of selective dopamine and norepinephrine autoreceptor and transporter inhibitors on catecholamine regulation in the OT.

As norepinephrine (NE) can exhibit similar electrochemical characteristics as DA (Park et al. 2009, Heien *et al.* 2003), and the ventral noradrenergic bundle (VNB), a major pathway of noradrenergic neurons, passes directly through the VTA/SN region (Ungerstedt 1971, Miyahara & Oomura 1982, Saphier 1993), electrical stimulation of this region may also activate the VNB and possibly evoke NE in the OT (Park et al. 2009, Park et al. 2010). Thus, to determine the identity of the major catecholamine in each OT subregion as well as its regulation via its autoreceptors and transporters, we used a previously established pharmacological criterion to distinguish DA from NE (Park et al. 2009, Park et al. 2011, Fox & Wightman 2017). Before drug administration (intraperitoneal (i.p.)), electrically evoked catecholamine in the OT at 60 Hz with 60 pulses were recorded every 4 or 5 min for a minimum of 30 min as a control, as described in previous studies (Park et al. 2010). If the electrically evoked maximal catecholamine concentration ($[CA]_{max}$) and half-decay ($t_{1/2}$) changed over 20% over 30 min during control recordings, we waited another 20–30 min until the evoked release was stabilized. Then, the NE α_2-adrenergic receptor antagonist, idazoxan (IDA, 3 mg/kg, i.p.), was administered and followed by the NE transporter inhibitor, desipramine (DMI, 15 mg/kg, i.p.), 30 min after IDA administration. Our previous studies showed that the maximal effects of both IDA and DMI on NE receptors and NET, respectively, took less than 20 min after their systemic administration (Herr et al. 2012, Park et al. 2009, Park et al. 2011). As shown as an individual example, IDA and DMI did not significantly alter the evoked catecholamine signal in any OT subregion 30 min after their administration (Fig. 2(a)). In contrast, in another set of experiments, the D2 receptor antagonist, raclopride (RAC, 2 mg/kg, i.p.) increased $[CA]_{max}$ and $t_{1/2}$ and the subsequent administration of the DAT inhibitor, GBR 12909 (GBR, 15 mg/kg, i.p.), further increased the evoked $[CA]_{max}$ and $t_{1/2}$ in all three subregions of the OT (Fig. 2(b)). It is noteworthy that the RAC effect on catecholamines maximizes within 20 min, while the maximum effects of GBR on DAT takes at least 40 min (Park et al. 2010, Budygin et al. 2000). Therefore, maximum changes of $[CA]_{max}$ and $t_{1/2}$ were recorded at 30 min and one hour after the systemic administration of RAC and GBR, respectively.

This trend was reflected in all subjects comprising the group mean of the drug effect (Fig. 2(c) & (d)). The average results from all animals show that only the D2 receptor and DAT specific drugs RAC and GBR significantly increased both $[CA]_{max}$ and $t_{1/2}$ from baseline levels. This strongly suggests that the major catecholamine in all of the OT subregions is DA. Therefore, the NE contribution to the electrically evoked DA in OT is negligible. This result also supports the hypothesis that both presynaptic D2 autoreceptors and the DAT play key roles in modulating DA release and removal, respectively, in the ventral striatum including the subregions of the OT. Interestingly, an analysis of the RAC effect on maximum evoked concentration revealed that this differed across the OT subregions (Two-way repeated measures ANOVA, Main effect of Region $F_{2,15} = 4.13$ and Drug $F_{1,15} = 58.8$, both $p < 0.05$) with RAC having a greater effect on the amOT compared to the alOT. However, the GBR effect on the evoked catecholamine concentration and $t_{1/2}$ was not significantly different between the OT subregions ($p > 0.05$).

Although naturally occurring phasic DA transients are rarely observed in anesthetized rats, spontaneous DA transients were clearly observed in the OT after the administration of the D2 and DAT inhibitors (Fig. 3). The average frequency and maximal concentration of DA transients are reported in Table 1. While all three subregions of the OT showed spontaneous transients after the administration of RAC and GBR, with similar frequencies of transients, their concentrations differed across the OT subregions (One-Way ANOVA, $F_{\mathbf{2,12}}$=4.13, $p < 0.05$), with the alOT subregion being lower than the amOT.

Comparison of DA dynamics in OT subregions.

Electrically evoked DA in the OT provides information on the dynamics of DA release and clearance. Representative examples of the time courses of DA in each of the three OT subregions are shown in Figure 4. DA release began immediately upon stimulus initiation, reached a maximum, and returned to its initial value after the stimulation (60 Hz, 60 pulses). Cyclic voltammograms recorded at the maximum were identical to DA (Fig. 4, insets) with its oxidation at ~+ 0.6 – +0.7 V and reduction at ~ −0.2 V – −0.3 V as described above. Both the average maximal DA concentration ($[DA]_{max}$) and the rise time to maximum DA concentration (t_r) evoked by electrical stimulation at 60 Hz was slightly less in the alOT when compared to the other subregions, although this effect did not reach significance ($[DA]_{max}$, $p = 0.07$ and t_r, $p = 0.055$; Table 2). However, the half-decay time ($t_{1/2}$), the time needed for DA to descend from its maximum to half of its value, was significantly different between each subregion (One-Way ANOVA, $F_{2,26}$=7.77, $p < 0.01$), with the amOT and pOT showing a significantly longer $t_{1/2}$ than the alOT ($p < 0.05$) indicating a more rapid clearance of evoked DA in the alOT.

Effects of the stimulation parameters on DA regulation in the OT.

The responses in each OT subregion to different stimulation parameters were investigated, as shown in Figure 5. Increasing stimulation frequency (5, 10, 20, 40, and 60 Hz, 60 pulses) showed that the amplitude increased in all three OT subregions, with an overall effect in average maximal responses ((Two-Way repeated measures ANOVA, Frequency: $F_{4,104}$ = 547), subregion ($F_{2,26}$ = 4.21) and a significant interaction ($F_{8,104}$ = 3.53, all $p < 0.05$))(Fig. 5(a) and (c)). While similar relative DA responses in the alOT and pOT at different stimulation frequencies were observed, the amOT showed greater relative responses than the other two subregions at lower frequencies (10 and 20 Hz). Steady-state responses were observed in all three OT subregions at 5 Hz (Fig. 5a and inset). Figure 5(b) and (d) show the responses in the three OT subregions to different pulse numbers (10, 20, 40 and 80 and 120 pulses at 60 Hz). Measurable responses (signal to noise (S/N) ≥ 5) were normally observed with at least 10 pulses at 60 Hz under these experimental conditions (Fig. 5b and inset). The response in the all three OT subregions increased linearly with pulse number, as evidenced by the pooled maximal response ($F_{5,105}$ = 1315), subregion ($F_{2,21}$ = 18.46) as well as a significant interaction ($F_{10,105}$ = 5.95, all $p < 0.05$)(Fig. 5(d)). In comparison to the other two regions, the relative response in the alOT showed greater maximal evoked DA levels between 10 and 80 pulses.

Discussion

The OT, as the ventral-most component of the ventral striatum, is a highly interconnected structure integrating information from both olfactory and diverse non-olfactory brain regions involved in a wide range of sensory and reward-related functions beyond that of odor processing (Wesson & Wilson 2011, Ikemoto 2007, Ikemoto 2003, Shin et al. 2010, Robinson et al. 2002, Robinson & Wightman 2004). Unlike other parts of the ventral striatum, the OT contains a distinct trilaminar structure consisting of a molecular (layer I), a dense cell layer (layer II), and a multiform layer (layer III) resembling cortical areas (Millhouse & Heimer 1984, Wesson & Wilson 2011). Moreover, there is a high degree of compartmentalization in the OT, including unique elements such as the Islands of Calleja, a sub-structure of granule cells forming reciprocal connections with the NAc, as well as specialized “dwarf cells” - small medium spiny neurons (MSNs) mainly observed in the deeper layers (I and II) of the OT (Hsieh & Puche 2013, Giessel & Datta 2014).

Recently, it has been shown that neurons in the OT in mice can encode both odor-based Pavlovian cue associations (Gadziola *et al.* 2015) and goal-directed licking behavior for natural reinforcers, and is sensitive to reward magnitude and type (Gadziola & Wesson 2016). Moreover, there is increasing evidence that distinct anatomical subregions of the OT, including the amOT, alOT, and pOT regions have distinct functional roles in both social odor-guided natural reinforcement (Agustin-Pavon et al. 2014, DiBenedictis et al. 2015), determining the appropriate response to cues associated with reward and punishment (Murata et al. 2015), and psychostimulant drug reward (Ikemoto 2007). This suggests that dopaminergic regulation in this brain area may differ from the other ventral striatal structures such as the NAc and also across different subregions of the OT, which may influence different behavioral responses. Indeed, while the OT receives strong mesolimbic DA input from the VTA like other ventral striatal compartments, the OT has a unique distribution pattern of DA receptors, DAT, and projection terminals from that of the neighboring NAc (Minuzzi & Cumming 2010, Giessel & Datta 2014, Ikemoto 2007, Hsieh & Puche 2013, Jansson *et al.* 1999). For example, although some have reported dense DAT expression in both the OT and the NAc (Ciliax *et al.* 1995), others have suggested that the density of the inhibitory autoreceptor D2/3 binding sites is less in the OT than in the NAc (Minuzzi & Cumming 2010). In this present study, we show for the first time that *in vivo* FSCV coupled with carbon-fiber microelectrodes can determine heterogeneous DA regulation in three subregions of the OT of anesthetized rats by monitoring rapid changes in DA concentration evoked by electrical stimulation of the VTA, despite the challenges presented by the small size and the relative anatomical inaccessibility of each region.

Neurochemical, electrochemical, and anatomical evidence confirms that major catecholamine in the OT is DA.

Electrical stimulation of the VTA can activate both DA cell bodies and the ventral noradrenergic bundle (VNB) that contains axons from NE cell bodies primarily from the nucleus of the solitary tract (A2) and other noradrenergic cell groups (A1, A5 and A7) (Ungerstedt 1971, Miyahara & Oomura 1982, Saphier 1993) resulting in increased NE concentration (Park et al. 2009, Park et al. 2011). Although the electrically evoked signal in

the OT showed the characteristic voltammograms of catecholamines like DA (Fig. 1 & 4 insets) and is identical to the voltammogram of DA found in the NAc and CPu (Park et al. 2009, Park et al. 2011), DA and NE are indistinguishable electrochemically (Park et al. 2009, Heien et al. 2003). This is a critical factor, as it has been established that NE contributes to the overall catecholaminergic signal in more posterior locations in other ventral striatal structures like the NAc shell, which is just above the OT (Park et al. 2010). Therefore, NE release in more posterior locations of the OT could be contributing to the changes in concentration observed during electrical stimulation, presenting a confound in our work as well as in previous data employing FSCV in the OT (Robinson et al. 2005, Robinson & Wightman 2004, Robinson et al. 2002). However, our pharmacological evidence suggests that the major catecholamine along both the anteroposterior and mediolateral extent of the OT evoked by the electrical stimulation of the VTA is DA.

Specifically, administration of selective NE autoreceptor and transporter inhibitors (IDA and DMI, respectively) in this study did not change the evoked DA signal in any subregion of the OT, while DA D2 receptor and transporter inhibitors (RAC and GBR, respectively) significantly increased the evoked DA concentration and its $t_{1/2}$ in the OT subregions (Fig. 2). Our findings are in agreement with previous neurochemical studies, which showed that over 94% catecholamine in the OT was DA, supporting the idea that evoked NE neurotransmission in the OT is minimal (Kilts & Anderson 1986, Kilts & Anderson 1987, Suaudchagny *et al.* 1989, Park et al. 2010, Ikemoto 2007, Seifert *et al.* 1998, Hsieh & Puche 2013, Mitchell *et al.* 1994). Nonetheless, as the VTA is a heterogeneous structure and also sends non-DA projection neurons such as GABA to the ventral striatal areas (Brown *et al.* 2012), which may also include the OT, the contribution of other neurons and neurotransmitter systems to the electrically evoked DA signal will need to be assessed further.

DA regulation in the subregions of OT is spatially distinct from neighboring limbic areas.

Our previous work demonstrated that FSCV could be used to selectively determine DA release evoked by optical stimulation of the VTA from both NAc and the amOT, and that the carbon-fiber microelectrode used for monitoring DA had sufficient spatial resolution to distinguish light evoked DA between the two compartments of the ventral striatum (Wakabayashi et al. 2016). This experimental approach revealed that evoked DA in the amOT was regulated differently compared with DA in the NAc. Our current study investigates electrically evoked DA regulation across three subregions, the amOT, alOT, and pOT. All three OT subregions are structurally much smaller than the NAc, CPu, and VP and consist of a region of evoked DA that is distinct from more dorsal areas anatomically associated with the NAc and the CPu (Fig. 1). The electrically evoked catecholamine in the VP where both DA and NE coexist was much less than the other brain regions. Consistent with previous work showing that electrically evoked catecholamines at a single, relatively posterior OT and NAc coordinate can be distinguished from each other using FSCV (Robinson et al. 2005), our results from multiple OT subregions across the anteroposterior and mediolateral axes demonstrate that FSCV can examine extracellular DA regulation in the OT without interference of NE and diffused DA from the NAc, CPu, or VP located immediately adjacent to the OT. Particularly, maximal evoked DA release was observed

within ~200 μm between layer I and II across all three OT subregions, where the dendrites of MSNs were mostly observed (Giessel & Datta 2014). For this study, the optimal depths of the bipolar stimulating electrode tips (spaced ~1.0 mm apart) used to evoke maximal DA release in the OT were around ~8.5 mm below the skull where maximal evoked DA release was also observed in the NAc and CPu (Park et al. 2009, Park et al. 2011). It should be noted that due to the relatively poor spatial resolution of electrical stimulation, a detailed examination of heterogeneous inputs of VTA neurons including DA neurons into the striatum and the OT will need to be conducted with higher spatial resolution techniques. However, under identical electrical stimulation conditions, the $[DA]_{max}$ in the OT was similar to that in NAc and CPu, but the rate of DA clearance in the OT was less than that of DA in the NAc and CPu. This is consistent with previous reports employing a range of methods (Annunziato *et al.* 1980, Horn *et al.* 1974, Robinson & Wightman 2004). This suggests that DA in the OT may have more time to diffuse further from its release sites, allowing DA in the OT to participate in "volume transmission" to a greater degree.

Although the results in the amOT are similar to our previous finding from optically evoked DA (Wakabayashi et al. 2016), electrically evoked $[DA]_{max}$ in the amOT showed a ~9 times greater amount of maximally evoked DA concentration (Table 2) when compared to optically evoked $[DA]_{max}$. This difference is in agreement with reports comparing electrically and optically evoked DA levels in the dorsal striatum and NAc after SN or VTA stimulation, respectively, in either *in vivo* or *in vitro* preparations (Bass *et al.* 2013, Bass *et al.* 2010). These differences are likely due to a combination of factors, including the possibility that electrical stimulation may stimulate more neurons due to its poor spatial resolution as described above in comparison to light stimulation. Unlike electrical stimulation, additional factors such as light transmittance influence the efficacy of light stimulation (Al-Juboori *et al.* 2013). Also, it should be noted that $[DA]_{max}$ evoked by optical stimulation depends on other factors not present with electrical stimulation, including the expression pattern of the non-native light sensitive channel used to excite the neuron and the position of the optical fiber delivering the light stimulation. Finally, electrical stimulation is comparatively non-specific, and readily stimulates fibers of passage in addition to cell bodies in the target region (Wakabayashi et al. 2016), while optical stimulation in the VTA would not stimulate fibers of passage originating from other, non-transfected parts of the brain (Cearley & Wolfe 2006). Taken together, these factors could explain some of the differences found between these two studies.

Heterogeneous DA regulation between subregions of OT.

The various stimulation parameters and pharmacological agents that we used revealed a significant difference in DA regulation between the subregions of the OT, as the rapid time resolution of the DA recordings at the carbon-fiber microelectrode enabled us to characterize the dynamics of release and uptake at a subsecond time resolution. Either inhibiting D2 autoreceptors or subsequently blocking the function of the DAT significantly altered DA dynamics in all three subregions, suggesting that extracellular DA in all three subregions is regulated by D2 autoreceptors and DAT. However, systemic administration of the D2 autoreceptor antagonist, RAC, increased the evoked $[DA]_{max}$ in the amOT more compared to the alOT and pOT, indicating that DA release in the amOT was more regulated by D2

receptors than the alOT and pOT. In contrast, the effect of RAC was smallest in the alOT, suggesting that there is comparatively less inhibition by D2 autoreceptors. Less autoreceptor inhibition in the alOT subregion could also explain why the alOT showed a greater relative DA release with increasing pulse number than the amOT and pOT (Fig. 5(d)). Additionally, there was significantly smaller $t_{1/2}$ of evoked DA under pre-drug control conditions in the alOT subregion compared to the other two subregions (Table 2). While this may initially suggest that DA is under greater regulation by DAT in the alOT, the effects of DAT blockade by GBR on maximal amplitude and half-decay time were not significantly different between the different OT subregions. Thus, this difference may instead result from less DA release in the alOT compared to the amOT and pOT (Table 2). In addition, previous immunohistochemistry studies have shown that VTA DA neuronal projections are more dense in the medial OT than in lateral parts of the anterior or posterior OT (Newman & Winans 1980).

The amOT showed a greater sensitivity to changes in stimulation frequency than the other subregions at 20 Hz (Fig. 5(c)). The characteristics of evoked DA release depend on three factors: the rapidity (frequency) of stimulation, the rate of DA clearance, and the amount release per impulse (Garris *et al.* 1997, Bergstrom & Garris 2003, Garris & Wightman 1994). Generally at lower stimulation frequencies, sufficient time exists for the release and uptake of DA to equalize to a steady-state level, while the shorter time between stimulus pulses at higher frequencies permits release to overtake clearance, resulting in peak-shaped signals largely dependent on the magnitude of DA release. Like the NAc and CPu, the evoked release of DA shows a steady-state release in all OT subregions at a low frequency, 5Hz (Fig. 5(a), inset). However, given that the amOT shows a significantly increased relative response to higher frequencies (10 and 20 Hz) compared to other subregions, these results suggest that amOT regulation of DA by inhibition of DA release and uptake via D2 autoreceptors and DAT, respectively, may be more readily overwhelmed at higher frequencies (> 5 Hz) compared to other regions of the OT.

Less spontaneous phasic DA transients in the alOT following inhibition of DA uptake and D2 autoreceptors.

While naturally occurring phasic DA transients in the NAc and OT are observed in awake rats as a result of burst firing of DA neurons in the VTA (Sombers *et al.* 2009, Wightman *et al.* 2007, Robinson et al. 2002, Robinson & Wightman 2004), similar transients are rarely seen in deeply anesthetized rats except under D2 receptor antagonism and DAT blockade (Venton & Wightman 2007, Park et al. 2010). These drugs increase burst firing and slow rhythmic oscillations in the firing rate of VTA DA neurons in anesthetized rats (Shi *et al.* 2004). The drug-induced spontaneous phasic DA transients have been observed in both the dorsal striatum (Venton & Wightman 2007) and ventral striatum (Park et al. 2011, Park et al. 2010, Wakabayashi et al. 2016). Here we report that while the frequency of the spontaneous transients does not differ across subregions, the maximal concentration of DA transients appears to be significantly smaller in the alOT than either the amOT or pOT (Table 1). Interestingly, when compared to drug-induced spontaneous DA transients in the NAc (frequency = 0.41 Hz and $[DA]_{max} = 0.18 \pm 0.04$ μM) (Park et al. 2011), amOT and pOT transients appear to be similar in $[DA]_{max}$, but all OT transients appear to be less frequent

and broader than those observed in the NAc (Fig. 3 & Supplementary Fig. 2). These indicate a longer half-decay time of DA transients although it is difficult to accurately evaluate the exact $t_{1/2}$ since individual transients were not always clearly resolved from each other. This may also reflect a difference in DA regulation via inhibitory autoreceptors and reuptake mechanisms in the OT, its subregions and NAc. These results may support increasing mechanistic evidence for a functional distinction in DA-related behaviors (e.g. natural and drug reward) between the NAc and the OT.

Conclusion

Taken together, our results in anesthetized rats show that heterogeneous DA regulation, primarily through differences in inhibitory autoreceptor regulation, differs in anatomical sub- territories of the OT. This difference in DA regulation may help explain some of the functional distinctions observed between the medial and lateral OT in both natural and drug reward (Ikemoto 2003, Agustin-Pavon et al. 2014, DiBenedictis et al. 2015) as well as switching between appropriate motivated behaviors in response to reward and danger (Murata et al. 2015). Moreover, as the VTA is not a uniform structure, ventral striatal DA regulation (i.e. OT subregions and the NAc) may depend on spatially heterogeneous input from the VTA (Ikemoto 2007). As electrical stimulation lacks spatial resolution, more localized stimulation approaches employing optogenetics may be beneficial in the future. As the first real-time DA recording in the subregions of the OT, the results of this study lay the groundwork for the future exploration of the role of DA in the OT in drug abuse and motivated behavior.

Supplementary Material

Refer to Web version on PubMed Central for supplementary material.

Acknowledgments and conflict of interest statement:

This work is supported by a start-up fund from the University at Buffalo-SUNY and SUNY Brain Network of Excellence Post-doctoral Fellow program. The authors report no biomedical financial interests or potential conflicts of interest.

List of abbreviations:

alOT	anterolateral olfactory tubercle
amOT	anteromedial olfactory tubercle
AP	anteroposterior
CA	catecholamine
CPu	caudate putamen
DA	dopamine
DAT	dopamine transporter

DMI	desipramine
DV	dorsoventral
FSCV	Fast Scan Cyclic Voltammetry
GBR	GBR-12909
IDA	idazoxan
i.p.	intraperitoneal
ML	mediolateral
MSN	medium spiny neuron
NAc	nucleus accumbens
NE	norepinephrine
NET	norepinephrine transporter
NST	nucleus of the solitary tract
OT	olfactory tubercle
pOT	posterior olfactory tubercule
SN	substantia nigra
Tris	tris(hydroxymethyl)aminomethane
VNB	ventral noradrenergic bundle
VTA	Ventral Tegmental Area
VP	ventral pallidum

References

Agustin-Pavon C, Martinez-Garcia F and Lanuza E (2014) Focal lesions within the ventral striato-pallidum abolish attraction for male chemosignals in female mice. Behav Brain Res, 259, 292–296. [PubMed: 24269269]

Al-Juboori SI, Dondzillo A, Stubblefield EA, Felsen G, Lei TC and Klug A (2013) Light scattering properties vary across different regions of the adult mouse brain. PloS one, 8, e67626. [PubMed: 23874433]

Alheid GF and Heimer L (1988) New perspectives in basal forebrain organization of special relevance for neuropsychiatric disorders: the striatopallidal, amygdaloid, and corticopetal components of substantia innominata. Neuroscience, 27, 1–39. [PubMed: 3059226]

Annunziato L, Leblanc P, Kordon C and Weiner RI (1980) Differences in the kinetics of dopamine uptake in synaptosome preparations of the median eminence relative to other dopaminergically inervated brain regions. Neuroendocrinology, 31, 316–320. [PubMed: 7442934]

Bass CE, Grinevich VP, Kulikova AD, Bonin KD and Budygin EA (2013) Terminal effects of optogenetic stimulation on dopamine dynamics in rat striatum. J Neurosci Methods, 214, 149–155. [PubMed: 23391758]

Bass CE, Grinevich VP, Vance ZB, Sullivan RP, Bonin KD and Budygin EA (2010) Optogenetic control of striatal dopamine release in rats. J Neurochem, 114, 1344–1352. [PubMed: 20534006]

Bergstrom BP and Garris PA (2003) "Passive stabilization" of striatal extracellular dopamine across the lesion spectrum encompassing the presymptomatic phase of Parkinson's disease: a voltammetric study in the 6-OHDA-lesioned rat. J Neurochem, 87, 1224–1236. [PubMed: 14622102]

Brown MT, Tan KR, O'Connor EC, Nikonenko I, Muller D and Luscher C (2012) Ventral tegmental area GABA projections pause accumbal cholinergic interneurons to enhance associative learning. Nature, 492, 452–456. [PubMed: 23178810]

Bucher ES and Wightman RM (2015) Electrochemical Analysis of Neurotransmitters. Annual review of analytical chemistry, 8, 239–261.

Budygin EA, Kilpatrick MR, Gainetdinov RR and Wightman RM (2000) Correlation between behavior and extracellular dopamine levels in rat striatum: comparison of microdialysis and fast-scan cyclic voltammetry. Neurosci Lett, 281, 9–12. [PubMed: 10686403]

Cahill PS and Wightman RM (1995) Simultaneous Amperometric Measurement of Ascorbate and Catecholamine Secretion from Individual Bovine Adrenal-Medullary Cells. Analytical Chemistry, 67, 2599–2605. [PubMed: 8849026]

Cearley CN and Wolfe JH (2006) Transduction characteristics of adeno-associated virus vectors expressing cap serotypes 7, 8, 9, and Rh10 in the mouse brain. Mol Ther, 13, 528–537. [PubMed: 16413228]

Ciliax BJ, Heilman C, Demchyshyn LL, Pristupa ZB, Ince E, Hersch SM, Niznik HB and Levey AI (1995) The dopamine transporter: immunochemical characterization and localization in brain. The Journal of neuroscience : the official journal of the Society for Neuroscie*nce*, 15, 1714–1723. [PubMed: 7534339]

DiBenedictis BT, Olugbemi AO, Baum MJ and Cherry JA (2015) DREADD-Induced Silencing of the Medial Olfactory Tubercle Disrupts the Preference of Female Mice for Opposite-Sex Chemosignals(1,2,3). eNeuro, 2.

Fox ME and Wightman RM (2017) Contrasting Regulation of Catecholamine Neurotransmission in the Behaving Brain: Pharmacological Insights from an Electrochemical Perspective. Pharmacol Rev, 69, 12–32. [PubMed: 28267676]

Gadziola MA, Tylicki KA, Christian DL and Wesson DW (2015) The olfactory tubercle encodes odor valence in behaving mice. The Journal of neuroscience : the official journal of the Society for Neuroscie*nce*, 35, 4515–4527. [PubMed: 25788670]

Gadziola MA and Wesson DW (2016) The Neural Representation of Goal-Directed Actions and Outcomes in the Ventral Striatum's Olfactory Tubercle. The Journal of neuroscience : the official journal of the Society for Neuroscie*nce*, 36, 548–560. [PubMed: 26758844]

Garris PA, Walker QD and Wightman RM (1997) Dopamine release and uptake rates both decrease in the partially denervated striatum in proportion to the loss of dopamine terminals. Brain Res, 753, 225–234. [PubMed: 9125407]

Garris PA and Wightman RM (1994) Different kinetics govern dopaminergic transmission in the amygdala, prefrontal cortex, and striatum: an in vivo voltammetric study. The Journal of neuroscience : the official journal of the Society for Ne*uroscience*, 14, 442–450. [PubMed: 8283249]

Giessel AJ and Datta SR (2014) Olfactory maps, circuits and computations. Current opinion in neurobiology, 24, 120–132. [PubMed: 24492088]

Heien ML, Phillips PE, Stuber GD, Seipel AT and Wightman RM (2003) Overoxidation of carbon-fiber microelectrodes enhances dopamine adsorption and increases sensitivity. Analyst, 128, 1413–1419. [PubMed: 14737224]

Herr NR, Park J, McElligott ZA, Belle AM, Carelli RM and Wightman RM (2012) In vivo voltammetry monitoring of electrically evoked extracellular norepinephrine in subregions of the bed nucleus of the stria terminalis. Journal of neurophysiology, 107, 1731–1737. [PubMed: 22190618]

Horn AS, Cuello AC and Miller RJ (1974) Dopamine in the mesolimbic system of the rat brain: endogenous levels and the effects of drugs on the uptake mechanism and stimulation of adenylate cyclase activity. J Neurochem, 22, 265–270. [PubMed: 4829953]

Hsieh YC and Puche AC (2013) Development of the Islands of Calleja. Brain Res, 1490, 52–60. [PubMed: 23122882]

Ikemoto S (2003) Involvement of the olfactory tubercle in cocaine reward: intracranial self-administration studies. The Journal of neuroscience : the official journal of the Society for Ne*uroscience*, 23, 9305–9311. [PubMed: 14561857]

Ikemoto S (2007) Dopamine reward circuitry: two projection systems from the ventral midbrain to the nucleus accumbens-olfactory tubercle complex. Brain Res Rev., 56, 27–78.. [PubMed: 17574681]

Jansson A, Goldstein M, Tinner B et al. (1999) On the distribution patterns of D1, D2, tyrosine hydroxylase and dopamine transporter immunoreactivities in the ventral striatum of the rat. Neuroscience, 89, 473–489. [PubMed: 10077329]

Kilts CD and Anderson CM (1986) The simultaneous quantification of dopamine, norepinephrine and epinephrine in micropunched rat brain nuclei by on-line trace enrichment HPLC with electrochemical detection: Distribution of catecholamines in the limbic system. Neurochem Int, 9, 437–445. [PubMed: 20493144]

Kilts CD and Anderson CM (1987) Mesoamygdaloid dopamine neurons: differential rates of dopamine turnover in discrete amygdaloid nuclei of the rat brain. Brain Res, 416, 402–408. [PubMed: 3620969]

Kita JM, Parker LE, Phillips PE, Garris PA and Wightman RM (2007) Paradoxical modulation of short-term facilitation of dopamine release by dopamine autoreceptors. J Neurochem, 102, 1115–1124. [PubMed: 17663751]

Michael DJ, Joseph JD, Kilpatrick MR, Travis ER and Wightman RM (1999) Improving data acquisition for fast scan cyclic voltammetry. Analytical Chemistry, 71, 3941–3947. [PubMed: 10500480]

Millhouse OE and Heimer L (1984) Cell configurations in the olfactory tubercle of the rat. J Comp Neurol, 228, 571–597. [PubMed: 6490970]

Minuzzi L and Cumming P (2010) Agonist binding fraction of dopamine D2/3 receptors in rat brain: a quantitative autoradiographic study. Neurochem Int, 56, 747–752. [PubMed: 20117160]

Mitchell K, Oke AF and Adams RN (1994) In vivo dynamics of norepinephrine release-reuptake in multiple terminal field regions of rat brain. J Neurochem, 63, 917–926. [PubMed: 8051568]

Miyahara S and Oomura Y (1982) Inhibitory-Action of the Ventral Noradrenergic Bundle on the Lateral Hypothalamic Neurons through Alpha-Noradrenergic Mechanisms in the Rat. Brain Research, 234, 459–463. [PubMed: 6277435]

Murata K, Kanno M, Ieki N, Mori K and Yamaguchi M (2015) Mapping of Learned Odor-Induced Motivated Behaviors in the Mouse Olfactory Tubercle. The Journal of neuroscience : the official journal of the Society for Neur*oscience*, 35, 10581–10599. [PubMed: 26203152]

Newman R and Winans SS (1980) An experimental study of the ventral striatum of the golden hamster. II. Neuronal connections of the olfactory tubercle. J Comp Neurol, 191, 193–212. [PubMed: 7410591]

Park J, Aragona BJ, Kile BM, Carelli RM and Wightman RM (2010) In vivo voltammetric monitoring of catecholamine release in subterritories of the nucleus accumbens shell. Neuroscience, 169, 132–142. [PubMed: 20451589]

Park J, Bucher ES, Budygin EA and Wightman RM (2015) Norepinephrine and dopamine transmission in 2 limbic regions differentially respond to acute noxious stimulation. Pain, 156, 318–327. [PubMed: 25599453]

Park J, Galligan JJ, Fink GD and Swain GM (2006) In vitro continuous amperometry with a diamond microelectrode coupled with video microscopy for simultaneously monitoring endogenous norepinephrine and its effect on the contractile response of a rat mesenteric artery. Analytical Chemistry, 78, 6756–6764. [PubMed: 17007494]

Park J, Kile BM and Wightman RM (2009) In vivo voltammetric monitoring of norepinephrine release in the rat ventral bed nucleus of the stria terminalis and anteroventral thalamic nucleus. Euro. J. of Neuro, 30, 2121–2133.

Park J, Takmakov P and Wightman RM (2011) In vivo comparison of norepinephrine and dopamine release in rat brain by simultaneous measurements with fast-scan cyclic voltammetry. J Neurochem, 119, 932–944. [PubMed: 21933188]

Paxinos G and Watson C (2007) The rat brain in stereotaxic coordinates. Academic Press/Elsevier, Amsterdam; Boston.

Rice ME and Patel JC (2015) Somatodendritic dopamine release: recent mechanistic insights. *Philosophical transactions of the Royal Society of* London. Series B, Biological sciences, 370.

Robinson DL, Heien ML and Wightman RM (2002) Frequency of dopamine concentration transients increases in dorsal and ventral striatum of male rats during introduction of conspecifics. The Journal of neuroscience : the official journal of the Society for *Neuroscience*, 22, 10477–10486. [PubMed: 12451147]

Robinson DL, Hermans A, Seipel AT and Wightman RM (2008) Monitoring rapid chemical communication in the brain. Chem Rev, 108, 2554–2584. [PubMed: 18576692]

Robinson DL, Volz TJ, Schenk JO and Wightman RM (2005) Acute ethanol decreases dopamine transporter velocity in rat striatum: in vivo and in vitro electrochemical measurements. Alcohol Clin Exp Res, 29, 746–755. [PubMed: 15897718]

Robinson DL and Wightman RM (2004) Nomifensine amplifies subsecond dopamine signals in the ventral striatum of freely-moving rats. J Neurochem, 90, 894–903. [PubMed: 15287895]

Robinson DL and Wightman RM (2007) Rapid Dopamine Release in Freely Moving Rats In: *Electrochemical Methods for Neuroscience*, (Michael AC and Borland LM eds.). Boca Raton (FL).

Saphier D (1993) Electrophysiology and neuropharmacology of noradrenergic projections to rat PVN magnocellular neurons. The American journal of physiology, 264, R891–902. [PubMed: 8388662]

Seifert U, Hartig W, Grosche J, Bruckner G, Riedel A and Brauer K (1998) Axonal expression sites of tyrosine hydroxylase, calretinin- and calbindin-immunoreactivity in striato-pallidal and septal nuclei of the rat brain: a double-immunolabelling study. Brain Res, 795, 227–246. [PubMed: 9622641]

Shi WX, Pun CL and Zhou Y (2004) Psychostimulants induce low-frequency oscillations in the firing activity of dopamine neurons. Neuropsychopharmacology, 29, 2160–2167. [PubMed: 15257309]

Shin R, Cao J, Webb SM and Ikemoto S (2010) Amphetamine administration into the ventral striatum facilitates behavioral interaction with unconditioned visual signals in rats. PloS one, 5, e8741. [PubMed: 20090902]

Sombers LA, Beyene M, Carelli RM and Wightman RM (2009) Synaptic overflow of dopamine in the nucleus accumbens arises from neuronal activity in the ventral tegmental area. The Journal of neuroscience : the official journal of the Society for Neuroscie*nce*, 29, 1735–1742. [PubMed: 19211880]

Suaudchagny MF, Buda M and Gonon FG (1989) Pharmacology of Electrically Evoked Dopamine Release Studied in the Rat Olfactory Tubercle by Invivo Electrochemistry. Eur J Pharmacol, 164, 273–283. [PubMed: 2788097]

Swamy BE and Venton BJ (2007) Subsecond detection of physiological adenosine concentrations using fast-scan cyclic voltammetry. Anal Chem, 79, 744–750. [PubMed: 17222045]

Ungerstedt U (1971) Stereotaxic mapping of the monoamine pathways in the rat brain. Acta Physiol Scand Suppl., 367, 1–48. [PubMed: 4109331]

Venton BJ and Wightman RM (2007) Pharmacologically induced, subsecond dopamine transients in the caudate-putamen of the anesthetized rat. Synapse, 61, 37–39. [PubMed: 17068772]

Voorn P, Jorritsma-Byham B, Van Dijk C and Buijs RM (1986) The dopaminergic innervation of the ventral striatum in the rat: a light- and electron-microscopical study with antibodies against dopamine. J Comp Neurol, 251, 84–99. [PubMed: 3760260]

Wakabayashi KT, Bruno MJ, Bass CE and Park J (2016) Application of fast-scan cyclic voltammetry for the in vivo characterization of optically evoked dopamine in the olfactory tubercle of the rat brain. Analyst, 141, 3746–3755. [PubMed: 27063845]

Wesson DW and Wilson DA (2011) Sniffing out the contributions of the olfactory tubercle to the sense of smell: hedonics, sensory integration, and more? Neuroscience and biobehavioral reviews, 35, 655–668. [PubMed: 20800615]

Wightman RM, Heien ML, Wassum KM et al. (2007) Dopamine release is heterogeneous within microenvironments of the rat nucleus accumbens. Eur J Neurosci, 26, 2046–2054. [PubMed: 17868375]

Zachek MK, Takmakov P, Park J, Wightman RM and McCarty GS (2010) Simultaneous monitoring of dopamine concentration at spatially different brain locations in vivo. Biosensors & Bioelectronics, 25, 1179–1185. [PubMed: 19896822]

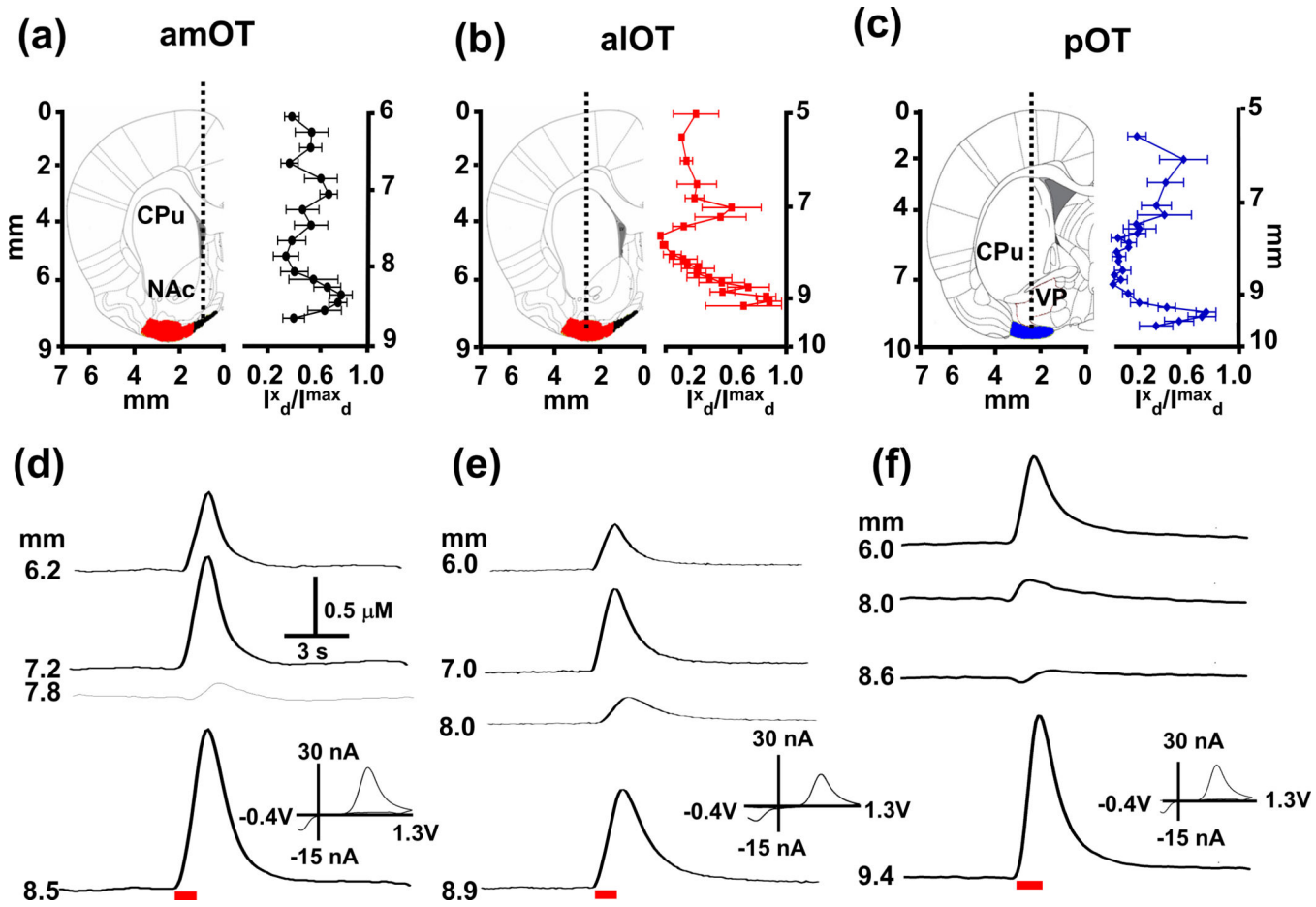

Figure 1.

Maps of electrically evoked catecholamine (CA) responses in the dorsal (CPu), ventral striatum (NAc), ventral pallidum (VP), and the amOT (a), alOT (b), and pOT (c) subregions as a function of the depth of the carbon-microelectrode. Panels (a)-(c) show coronal sections schematically (left, from Paxinos and Watson (Paxinos & Watson 2007)). The approximate path of the microelectrode (left, dotted line) was aimed at the different subregions of the OT (black: amOT, red: alOT, blue: pOT)(left). Relative response of catecholamine in the OT subregions are shown on the right. Mean relative response (I^x_d/I^{max}_d) of catecholamine in response to VTA electrical stimulation (60 Hz, 60 pulses) in the amOT (n=6), alOT (n=5), and pOT (n = 8) subregions at different depths of the microelectrode where I^x_d is the response at a particular depth divided by the maximal response, I^{max}_d of catecholamine. Panels (d)-(f) show representative CA concentration versus time traces at different depths of the microelectrode for each OT subregion before, during and after the electrical stimulation; insets show the distinct cyclic voltammogram for CA at the peak concentration values. Red bar denotes electrical stimulation of the VTA/SN interval (60 Hz, 60 pulses). Abbreviations used: CPu, caudate-putamen; NAc, nucleus accumbens; OT, olfactory tubercle; VP, ventral pallidum.

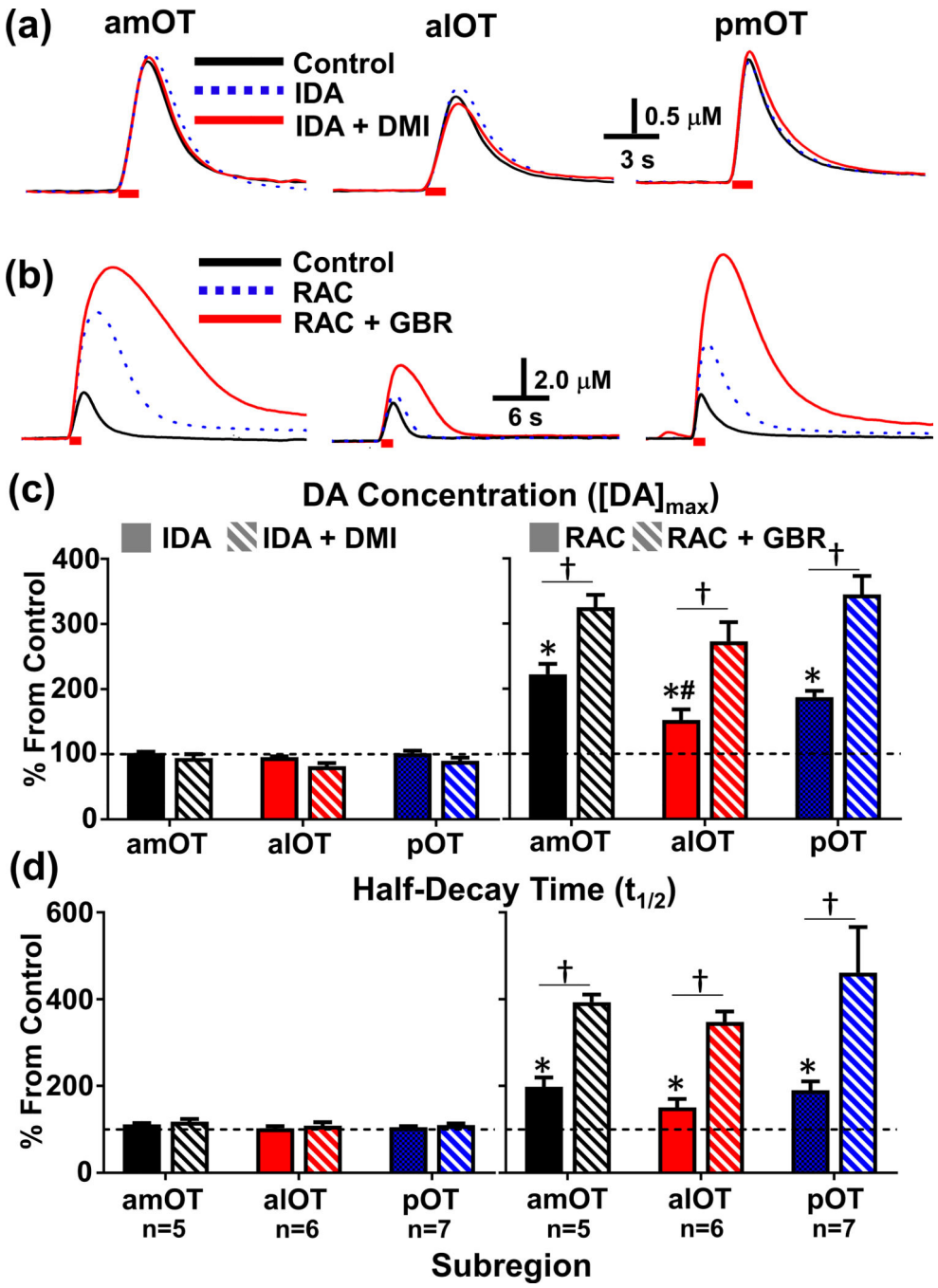

Figure 2.

Effect of selective NE and DA autoreceptor and transporter inhibitors on electrically evoked release and uptake in the subregions of the OT. The NE drugs, idazoxan (IDA, 3 mg/kg, dotted blue line), and IDA + desipramine (DMI, 15 mg/kg, solid read line) did not alter release or uptake in the representative examples of evoked release in all of the subregions of the OT (a). In contrast, a D2 receptor antagonist, raclopride (RAC, 2m/kg, dotted blue line) increased both $[CA]_{max}$ and $t_{1/2}$ in the representative examples of evoked release in all of the OT subregions (b). Subsequent administration of a DAT inhibitor, GBR 12909 (GBR, 15

mg/kg, solid red line) potentiated both $[CA]_{max}$ and $t_{1/2}$ in the subregions of the OT. Red bar indicates the duration of the electrical stimulation of the VTA (60 Hz, 60 p). Effect of the these agents on the average maximum evoked catecholamine concentration ($[CA]_{max}$) and half-decay time ($t_{1/2}$) in the OT subregions; the NE drugs idazoxan (IDA, 3 mg/kg, i.p.) and IDA + desipramine (DMI, 15 mg/kg, i.p.) had no significant effect on either the $[CA]_{max}$ (c, left) or the $t_{1/2}$ (d, left). Raclopride (RAC, 2 mg/kg, i.p.) significantly increased evoked $[CA]_{max}$ ((c, right), amOT t_4=7.61, alOT t_5=3.16, pOT t_7=8.94, *, all $p < 0.0001$) and half-decay time ((d, right), amOT t_4=4.54, alOT t_5=2.66, pOT t_6=4.37, all $p < 0.05$) from pre-drug control levels (dashed line). Subsequent administration of GBR 12909 (GBR, 15 mg/kg, i.p.) after RAC further increased maximum evoked release from baseline levels. Fisher post-hoc tests revealed that the $[CA]_{max}$ after RAC was greater in the amOT than in the alOT (#, $p < 0.05$), and that the effect of RAC+GBR on maximum evoked release was greater than RAC alone for all OT subregions (†, $p < 0.05$). GBR after RAC also increased $t_{1/2}$ from baseline levels (two-way repeated measures ANOVA, main effect of drug $F_{1,15}$=41.9, $p < 0.0001$), although this effect was not statistically different across OT subregions.

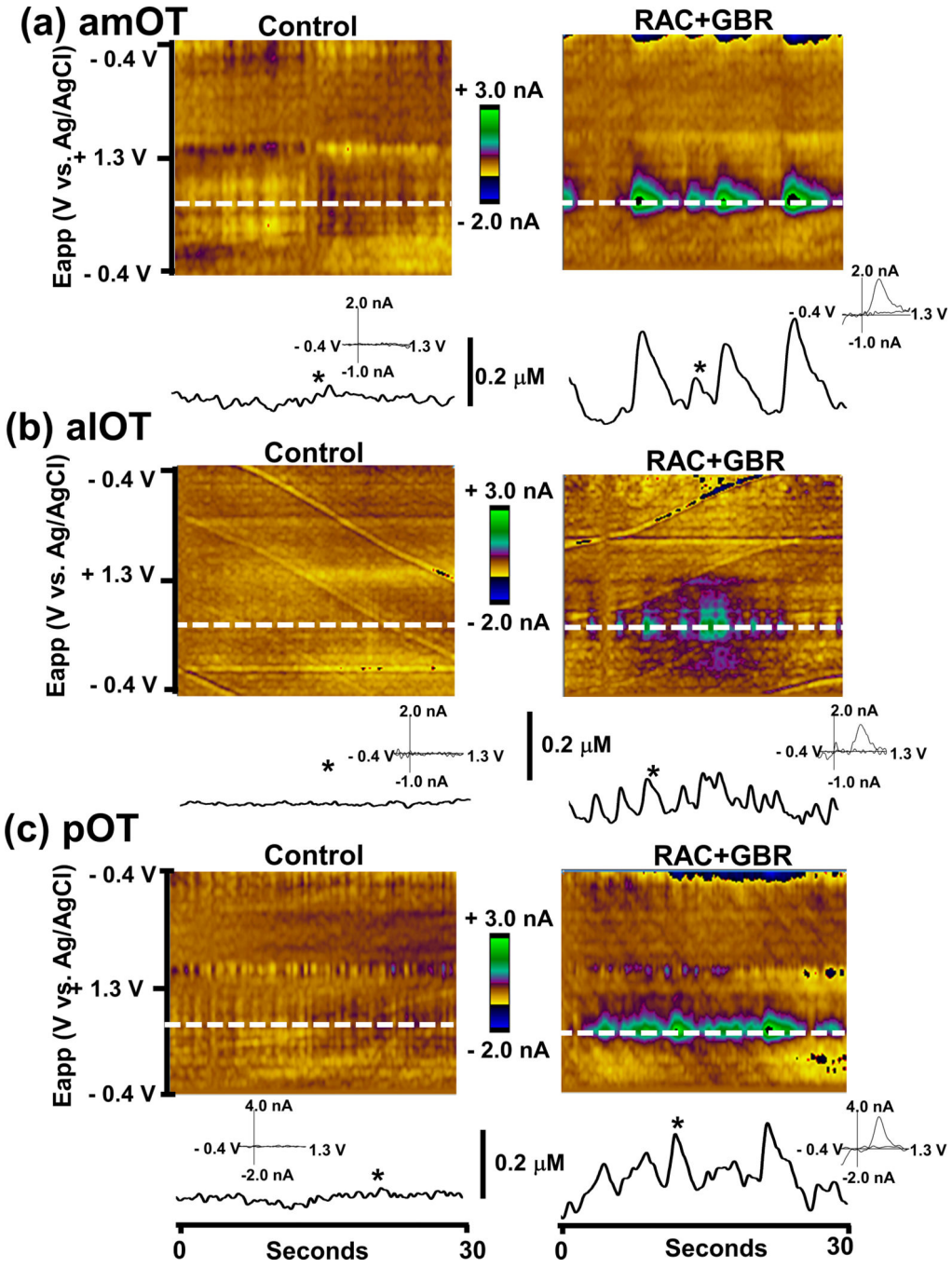

Figure 3.

Combined inhibition of DA uptake and D2 antagonism induces spontaneous DA transients in all subregions of the OT. Color plot representations of background-subtracted cyclic voltammograms collected over 30s before (left) and after (right) raclopride (RAC, 2 mg/kg, i.p.) and GBR 12909 (GBR, 15 mg/kg, i.p.) administration. DA concentration changes were seen in the color plot at the potential for DA oxidation (~ 0.6 – 0.7 V, dashed white line). The time courses of the DA concentration changes are shown below each color plot. Cyclic voltammograms are shown as insets recorded at the time indicated by the asterisk (*).

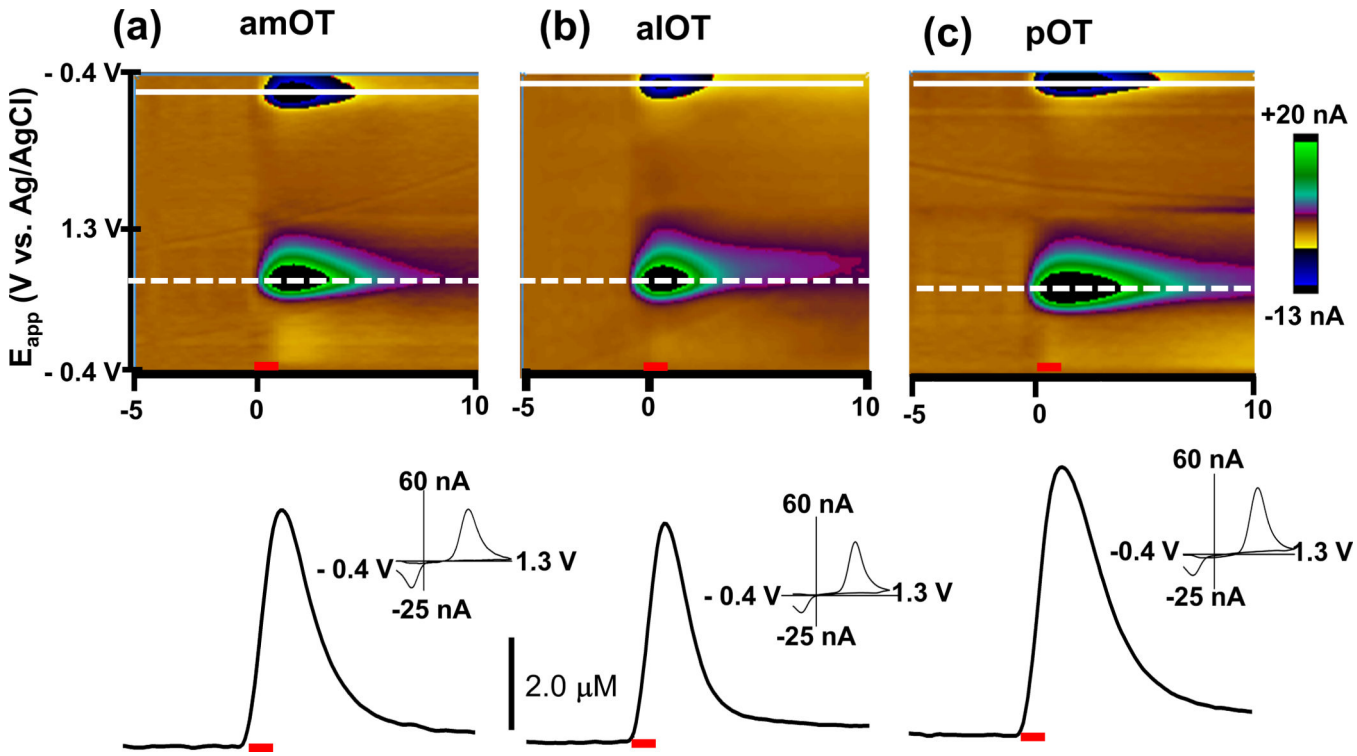

Figure 4.

Comparison of electrically evoked DA regulation in subregions of the OT. Representative examples of the change in DA concentration in the OT (amOT (a), alOT (b), pOT (c)) after stimulation (60 Hz, 60 pulses) of the VTA. Upper panels are color plots for the voltammetric data shown for each example, comprised of all background-subtracted cyclic voltammograms recorded for 5 s before and 10 s after stimulation, with current changes encoded in false color. Changes in DA concentration occurred at the potential for its oxidation (~+0.6 - +0.7 V, dotted line) and reduction (~ −0.3 - −0.2 V, solid line). Lower plots show changes in DA concentration before, during and after stimulation, shown at the potential where DA is oxidized. Background-subtracted cyclic voltammograms are shown as insets at the maximum of evoked release. The red bars indicate the period of electrical stimulation.

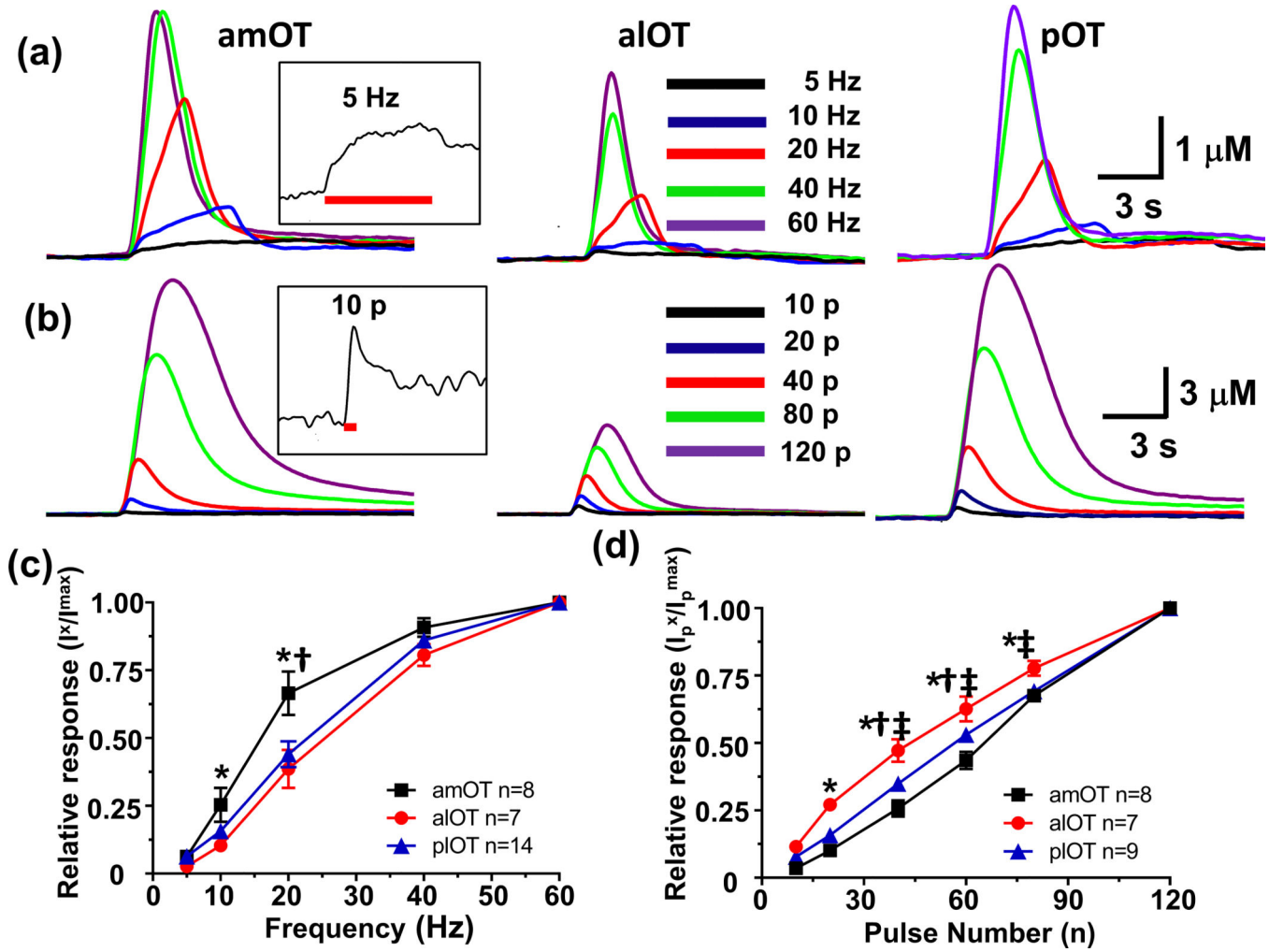

Figure 5.

Comparison of representative DA responses in the amOT, alOT and pOT subregions as a function of frequency (a) and pulse number (b). Representative evoked DA concentration traces at 5 Hz and 10 pulses are shown as insets, in (a) and (b), respectively. Maximal mean DA responses in the subregions of the OT as a function of frequency (c) and pulse number (d) as shown as relative response (monitored DA response (I^x)/maximal response (I^{max})). Significantly different response between the alOT and amOT (*), amOT and pOT (†), alOT and pOT (‡) subregions ($p < 0.05$).

Table 1.

Characteristics of spontaneous DA transients after the systemic administration of RAC and GBR in subregions of the OT.

Subregion (n = 5)	Frequency (Hz)	$[DA]_{max}$ (μM)
amOT	0.22 ± 0.02	0.25 ± 0.06 *
alOT	0.18 ± 0.02	0.09 ± 0.02 *
pOT	0.17 ± 0.03	0.17 ± 0.02

* indicates significant difference via Fisher's Post-hoc test ($p < 0.05$).

Frequency of naturally occurring phasic DA transients given as Hz (number of transients per second). $[DA]_{max}$ is the average maximal DA concentration of spontaneous transients. Values represent the mean ± SEM.

Table 2.

Numerical parameters measured from evoked DA in the subregions of the OT after electrical stimulation (60 Hz, 60 p).

Subregion	$[DA]_{max}$ (μM)	t_r (s)	$t_{1/2}$ (s)
amOT (n=7)	2.89 ± 0.43	1.63 ± 0.10	1.84 ± 0.19
alOT (n=10)	2.01 ± 0.15	1.33 ± 0.04	1.27 ± 0.05 *,†
pOT (n=12)	3.00 ± 0.35	1.50 ± 0.09	1.83 ± 0.12

*,† indicate significant difference ($p < 0.05$) between alOT and amOT, alOT and pOT, respectively.

$[DA]_{max}$ is the maximally evoked DA concentration, t_r is the time required to reach $[DA]_{max}$ from the start of the stimulation, and $t_{1/2}$ is the time required for $[DA]_{max}$ to decay to 50% of its value. Values represent the mean ± SEM and were compared by One-Way ANOVA followed by a Fisher post-hoc test.